

Charge separation at disordered semiconductor heterojunctions from random walk numerical simulations†

Cite this: *Phys. Chem. Chem. Phys.*, 2014, 16, 4082

Humberto J. Mandujano-Ramírez,^a José P. González-Vázquez,^{*b} Gerko Oskam,^a Thomas Dittrich,^c Germa Garcia-Belmonte,^d Iván Mora-Seró,^d Juan Bisquert^d and Juan A. Anta^{*b}

Many recent advances in novel solar cell technologies are based on charge separation in disordered semiconductor heterojunctions. In this work we use the Random Walk Numerical Simulation (RWNS) method to model the dynamics of electrons and holes in two disordered semiconductors in contact. Miller–Abrahams hopping rates and a tunnelling distance-dependent electron–hole annihilation mechanism are used to model transport and recombination, respectively. To test the validity of the model, three numerical “experiments” have been devised: (1) in the absence of constant illumination, charge separation has been quantified by computing surface photovoltage (SPV) transients. (2) By applying a continuous generation of electron–hole pairs, the model can be used to simulate a solar cell under steady-state conditions. This has been exploited to calculate open-circuit voltages and recombination currents for an archetypical bulk heterojunction solar cell (BHJ). (3) The calculations have been extended to nanostructured solar cells with inorganic sensitizers to study, specifically, non-ideality in the recombination rate. The RWNS model in combination with exponential disorder and an activated tunnelling mechanism for transport and recombination is shown to reproduce correctly charge separation parameters in these three “experiments”. This provides a theoretical basis to study relevant features of novel solar cell technologies.

Received 8th October 2013,
Accepted 9th December 2013

DOI: 10.1039/c3cp54237h

www.rsc.org/pccp

Introduction

The photovoltaic performance of solar cells depends on the efficient realization of several subsequent internal processes, from photon absorption to final collection of charge carriers at external contacts. Among all of them, one of the most critical points consists of the separation of photogenerated charge carriers. The open-circuit photovoltage (V_{oc}) of a solar cell is limited by the diode saturation current density, and it is affected by the extent of charge separation and by the rates of charge transport and recombination of carriers in the solar cell. The diode saturation current density, and the ideality factor m , can be given analytically for an ideal p–n junction,¹ but not for a

disordered heterojunction. Hence, more developed approaches are required for a deeper understanding of limiting processes.

Disordered heterojunctions are important in new generation solar cells such as a-Si:H solar cells, heterojunction with intrinsic thin film solar cells² (HIT), bulk heterojunction solar cells^{3,4} (BHJ) or quantum dot sensitized solar cells^{5,6} (QDSC). Recently record efficiencies have been reported for devices made of nanostructured TiO₂ solar cells sensitized with an inorganic perovskite,⁷ which is found to act as both a sensitizer and a semiconductor.^{8,9} The use of a disordered material offers advantages such as a simpler fabrication procedure, but also causes additional energy losses, associated with the presence of a broad distribution of energy localized states or traps.¹⁰ This distribution is observed to be exponential, defined by a trap density N_t and a characteristic temperature T_0 . Hence, in addition to band alignment, explicit consideration of this intrinsic disorder for two semiconductors in contact and its influence on diffusion and recombination is required to describe charge separation in this type of solar cells.

Currently, many experimental techniques are commonly used to study electronic processes in new generation heterojunction solar cells. Among them, dynamic measurements that allow us to study transport and recombination mechanisms in detail are very important, since they give information about time constants of

^a Departamento de Física Aplicada, CINVESTAV-IPN, Mérida, Yucatán 97310, México

^b Área de Química Física, Universidad Pablo de Olavide, Sevilla, Spain.
E-mail: jpgonzalez@upo.es, anta@upo.es

^c Helmholtz-Zentrum Berlin für Materialien und Energie, Glienicke Str. 100, D-14109 Berlin, Germany

^d Photovoltaic and Optoelectronic Devices Group, Departament de Física, Universitat Jaume I, ES-12071 Castelló, Spain

† Electronic supplementary information (ESI) available. See DOI: 10.1039/c3cp54237h

elementary steps. This is the case of surface photovoltage (SPV) analysis and electrochemical impedance spectroscopy (EIS).

SPV analysis is particularly useful when considering charge separation at very short distances.^{11–16} In the most general case, a SPV transient can be expressed by¹⁶

$$\text{SPV}(t) = \frac{q}{\varepsilon\varepsilon_0} N(t) (\langle x_p \rangle(t) - \langle x_n \rangle(t)) \quad (1)$$

where q is the elementary charge, ε is the dielectric constant, ε_0 is the vacuum permittivity, $N(t)$ is the total amount of electron-hole pairs per unit area at time t and $\langle x_{p(n)} \rangle(t)$ is the mean position of holes (electrons). Dynamic measurements are very important since they allow us to study transport and recombination mechanisms in more detail.

On the other hand, EIS has been shown to be a very useful approach.¹⁷ This technique allows us to gain insight into loss mechanisms from the measurements of the recombination resistance R_{rec} of the device, which is defined as the derivative of the carrier recombination current J_{rec} .

$$R_{\text{rec}} = \frac{1}{L} \left(\frac{\partial J_{\text{rec}}}{\partial V_F} \right)^{-1} \quad (2)$$

where L is the active layer thickness and V_F the voltage drop across the device. The recombination current J_{rec} is likewise expressed as a function of the voltage as

$$J_{\text{rec}} = J_0 \exp\left(\frac{\beta q V_F}{k_B T}\right) \quad (3)$$

where J_0 is the reverse current, k_B the Boltzmann constant, and T the temperature of the system. The parameter β , corresponding to the inverse of the ideality factor ($\beta = 1/m$) of the JV characteristics, is found to be equal to that appearing in the relationship between the open-circuit voltage and the illumination intensity,¹⁸

$$V_{\text{oc}} \propto \frac{k_B T}{\beta q} \ln I \quad (4)$$

EIS recombination resistance measurements and fitting to eqn (2) and (3) readily yield the parameter β and the ideality factor of the solar cell.

Nevertheless, interpretation of both types of experiment in a disordered heterojunction is not straightforward due to the simultaneous influence of many processes.¹⁹ For this reason, the development of appropriate modeling techniques that permit rigorous and reliable fundamental knowledge is needed. Significant progress has already been achieved in this context. For example, in several theoretical publications in the field of BHJ solar cells, recombination features have been analyzed in terms of the distribution of localized states,²⁰ the role of traps in the charge transfer processes²¹ or the specific morphology of the device.²² Likewise, for solar cells sensitized with inorganic semiconductors, the influence of energy disorder on interfacial processes occurring in both the light absorber⁵ and in the electrolyte²³ has been addressed. Examination of the behavior of the β -parameter as obtained by impedance spectroscopy has been carried out in several reports in the context of dye-sensitized solar cells (DSC)^{19,24} and BHJ solar cells.¹⁸

However, analytical approaches seem to be incomplete in many cases due to the complexity of disordered heterojunction systems. They often present limitations when considering essential relationships between critical properties, such as morphology, anisotropy or percolation effects. Thus, numerical and “molecular” simulations are presented as suitable alternative methods for the description of those features and some studies have already been accomplished in the context of disordered organic media^{25–27} and HIT solar cells.²⁸

This work intends to contribute in this sense by proposing a general model of a disordered semiconductor heterojunction that *explicitly* considers charge transport and recombination mechanisms. The model allows the consideration of energy disorder from first principles, *i.e.*, from basic assumptions about charge dynamics on the nanoscale. Moreover, the model presented here is specifically designed to permit a direct comparison of the results with experimental measurements obtained by SPV transients or EIS, which aims to interpret experimental magnitudes in terms of microscopic parameters.^{29,30}

It is important to make clear that the results presented in this work are based on the following assumptions: (1) an exponential functionality has been assumed to model energy disorder, (2) an activated tunnelling mechanism based on Miller–Abrahams hopping rates has been used to model transport and recombination, (3) Coulombic effects are considered negligible, and (4) no external contacts are introduced in the numerical calculations.

With regard to (1) the exponential density of states has been shown to model BHJ solar cells³¹ and sensitized nanostructured solar cells reasonably well.^{30,32} Although a Gaussian distribution has been used more widely in the context of organic semiconductors,²⁵ in many cases a Gaussian tail and an exponential distribution are not easily distinguished and result in the same experimentally observed tendencies.^{31,33,34} Concerning (2), the hopping model is a well accepted mechanism in organic semiconductors^{25,35,36} but it has also been shown to be consistent with the empirical phenomenology in solar cells made of inorganic nanostructured semiconductors: although the trap-limited transport method is generally used, the hopping dynamics result in identical experimental tendencies except for under rather extreme circumstances.³⁷

In connection to (3), electrical fields are known not to have a significant effect in sensitized nanostructured inorganic solar cells.³⁸ Furthermore, it has been recently shown that the experimental transport kinetics of typical BHJ solar cells can also be explained without the presence of an internal electrical field.³⁷ Finally, regarding (4), no external contacts are incorporated in our numerical calculations. This is in principle the simplest choice to model SPV experiments, but it also provides a first approximation for the V_{oc} of complete cells if the Fermi level of both electrons and holes can be considered equilibrated with their external contacts.

Although choices different from (1)–(4) could be considered, we have focused on these in order to obtain a unified description, and because relevant features of solar cells based on disordered heterojunctions are correctly reproduced. Obviously the model allows for easy implementation of other densities of states or transport mechanism, in order to reproduce more specific

situations. In this regard, modelling applications for particular cases are underway in the group.

Methodology

The RW simulation method^{40–43} is a stochastic calculation in which particles are moved at random in a 3-dimensional network of traps arranged on a lattice that is not necessarily ordered. The use of RW methods, also called Monte Carlo, to study charge transport in disordered materials goes back to the early eighties, mainly due to the studies of Movaghar, Bäessler, Baranovskii and coworkers.^{44–47} Later on, the Continuous Time Random Walk (CTRW) theory of Scher and Montroll was adapted to model nanostructured solar cells, thanks to the RW algorithm that sampled efficiently the trap energy distribution characteristics of nanocrystalline TiO₂.⁴⁰ Since then, RW calculations have been used to study electron mobilities,³⁴ diffusion coefficients^{41,48,49} and recombination properties^{50–52} in dye-sensitized solar cells. Recently, the kinetic Monte-Carlo technique has also been used successfully to model device performance in BJJ solar cells.^{22,26,27}

For the purpose of the present work, in the context of a RW simulation, a disordered interface has been implemented to construct a semiconductor heterostructure. This has been done by separating the network of traps into two parts, in order to define each part as a different semiconductor. Thus, along with a specific spatial configuration, to each part an energy distribution of traps for both electrons and holes is assigned, such that four different energy trap distributions are present in the calculation, all of them defined by a mobility edge, which defines the band position, and a degree of energy disorder. One important feature of this method is that it allows us to define an arbitrary energy distribution easily, which is a clear advantage when studying the effect of disorder on the performance of new generation solar cells. However, in this work, as explained in the introduction, we have assumed that energies of the traps are distributed according to an exponential function.^{53–55} Since two types of charge carrier are considered simultaneously, we have used the following expressions for the energy dependence of the density of electrons and holes, respectively

$$\begin{aligned} g_n(E) &= \frac{N_1}{k_B T_{0n}} \exp[(E - E_c)/k_B T_{0n}] \\ g_p(E) &= \frac{N_1}{k_B T_{0p}} \exp[(E_v - E)/k_B T_{0p}] \end{aligned} \quad (5)$$

where $N_1 (= 1/a_1^3)$ is the total trap density, a_1 is the average trap distance, $T_{0,n(p)}$ is the characteristic temperature of the distribution⁵⁶ for electrons (holes), E is the trap energy and $E_c(v)$ is the electron (hole) mobility edge. By defining adequate mobility edges, specific band alignments can be systematically studied. A schematic representation of the model is shown in Fig. 1.

The numerical procedure runs as follows. Electrons and holes are initially placed at random on the network of traps of one of the semiconductors acting as absorber material (initial pair density: n_0). Each carrier is then given a certain detrapping time that determines the jumping rate or probability of a carrier to jump to another site. If we assume a hopping mechanism^{45,53} of

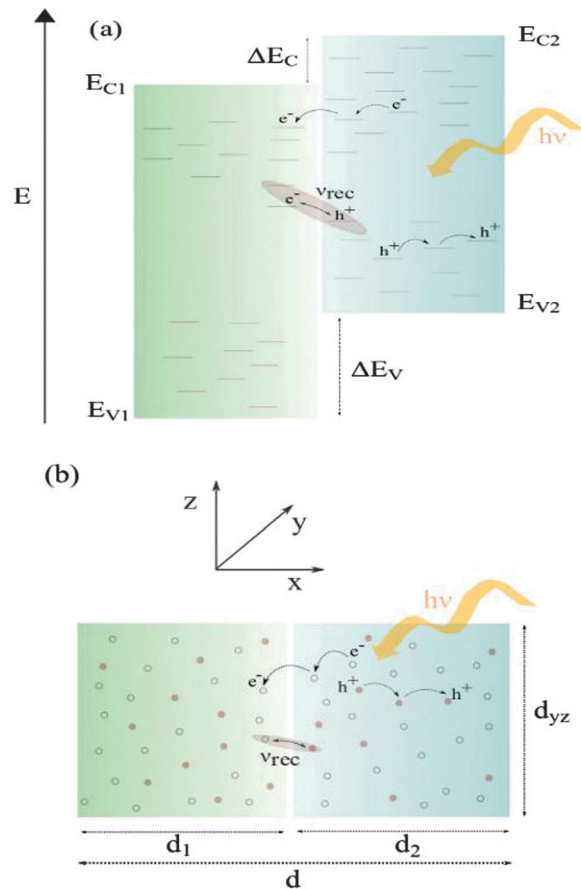


Fig. 1 Illustration of the disordered semiconductor heterojunction model studied in this work. The disordered heterojunction is modeled by means of band-offset energy distributions of localized states for both electrons and holes. In the left picture (a) the heterojunction is represented on the energy scale. In the right picture (b), the geometrical features of the random walk model are shown. A hopping transport model is used for detrapping times (or rates). See the text for more details.

transport, the detrapping or release time for a carrier jumping from a trap i to a trap j is obtained from the following equation

$$t_{ij} = -\ln(R)t_0 \exp\left(\frac{2r_{ij}}{\alpha_1} + \frac{E_j - E_i + |E_j - E_i|}{2k_B T}\right) \quad (6)$$

where t_0 is the inverse of the attempt-to-jump frequency, α_1 is the localization radius, r_{ij} is the distance between the traps and E_i and E_j are the energies of the starting and target traps, respectively. In analogy to this approach, to account for electron–hole annihilation, a distance dependent recombination probability is introduced in the computation. Here we assume that there is a tunneling mechanism in such a way that charge carriers present in different traps are allowed to recombine with each other due to an overlap of the wave functions of separated electrons and holes. Hence, we use the following equation to account for recombination times³¹

$$t_r = -\ln(R)t_{r0} \exp\left(\frac{2r_{np}}{\alpha_0}\right) \quad (7)$$

where t_{r0} is the inverse of a recombination frequency, α_0 is the recombination radius and r_{np} is the distance between electrons

and holes. As it will be shown below both t_{r0} and α_0 have a strong influence on the degree of charge separation, as they control the recombination loss, both in time and distance. Hence, they are fitting quantities that provide key information about the recombination rate and the distance range in which recombination events take place.

It must be noted that there is no energy-dependent factor in eqn (7). We have followed here ref. 31 and assumed that the recombination process is analogous to the hopping process and that electron–hole recombination is always a process where energy is emitted, either radiatively or non-radiatively *via* interaction with phonons. However, energy dependences are expected to be important, as predicted, for instance, from the Marcus model.^{22,57} For instance, it has been shown recently that a low reorganization energy for interface charge transfer is one of the paths for higher efficiencies in organic solar cells.⁵⁸ For simplicity, in this work we have assumed that the recombination simulation time is energy independent. Other authors have also neglected explicit energy contributions in the recombination process with good results.^{25,59} We will see below that this simple model can reproduce many experimental features typically observed in solar cells based on disordered heterojunctions.

Once charge carriers have been injected, hopping and recombination times are computed for both electrons and holes *via* eqn (6) and (7), respectively. Both types of times are then stored in a list of waiting times in such a way that if the minimum time t_{\min} is a detrapping time, the corresponding carrier is then moved into its target site, whereas if it is a recombination time, the corresponding electron–hole pair is removed from the sample. (Note that several choices for jump or recombination events are possible, depending on the distance and/or the energy difference, but only the event with the shortest waiting time is picked up.) Once the jump or the recombination event has been completed, the hopping and recombination times of the rest of the carriers are reduced by t_{\min} . The same procedure is repeated in each simulation step such that the jump or electron–hole recombination event with the minimum waiting time is executed. As stated in the introduction, no external contacts are considered, so periodic boundary conditions along the y – z direction are applied. Thus, a carrier crossing a y – z boundary is automatically reinjected through the opposite side of the box. In contrast, we impose reflecting boundary conditions in the x -dimension such that carriers arriving at a boundary in this direction are bounced back and continue to move across the network of sites. The thickness of each material can therefore be introduced arbitrarily.

Using this procedure, charge separation is expected to occur from the random walk of charge carriers when a favourable band alignment is implemented. In this work, we have carried out two types of RW simulation: (1) transient simulations and (2) steady-state simulations. For the first type, injection of electron–hole pairs is only considered at the beginning of the simulation, hence, electrons and holes are expected to undergo successive recombination events until all of them have been removed. For this case we have quantified charge separation by monitoring the time evolution of the SPV^{11,29,30} using eqn (1). Thus, the procedure consists of computing SPV histograms from the mean positions of

electrons and holes at each time in the RW simulation. Dynamic simulation experiments of SPV transients are needed for getting the order of magnitude of t_0 and the role of band offsets.

On the other hand, steady state simulations have also been carried out, in which a continuous injection of electron–hole pairs is explicitly considered according to the photon absorption rate. Specifically, the frequency of charge injection events is determined from the illumination under AM1.5G conditions (1000 W m⁻² of integrated power density), which yields a generation rate of $G = 7.5 \times 10^{16}$ cm⁻² s⁻¹.⁶⁰ Thus, this value, along with the dimensions of the simulation box, allows us to compute the *generation time*, t_G , that separates two correlative generation events during the simulation. For instance, for a 25 nm × 25 nm × 25 nm box $t_G = 2.1 \times 10^6 t_0$, whereas for a 50 nm × 50 nm × 50 nm box it is four times shorter.

As mentioned above, reflecting boundaries in the x -dimension are applied, which is a strong approximation to simulate the cell. However, we assume that at open-circuit and for good (ohmic) contacts, the densities of electrons and holes are only determined by generation and recombination across the interface. Hence, the impact of using reflecting boundaries on the charge separation parameters is expected to be low.

The purpose of steady-state simulations is to determine magnitudes under steady-state conditions rather than studying the process of charge separation in itself. For this reason, holes and electrons are injected into different semiconductors in the heterojunction. This assumption is made to allow the stationary state to be reached more rapidly thereby avoiding too large computational times. As we will see below, charge separation is adequately reproduced in transient simulations. Therefore, by starting the simulation from a situation in which electrons and holes are already separated, we save computation time and we can obtain steady-state properties with better statistics.

A steady-state situation is expected to be reached in this second type of simulations as a consequence of balance between generation and recombination. This is verified by an occupation probability according to Fermi–Dirac statistics as well as a constant number of “alive” electron–hole pairs during the simulation. Consequently, well-defined Fermi levels can be obtained in both semiconductors. Hence, following Bisquert and Garcia-Belmonte,³⁹ we can compute the open-circuit voltage from

$$V_{oc} = \frac{1}{q} (E_{Fn}^2 - E_{Fp}^1) \quad (8)$$

where E_{Fn}^2 and E_{Fp}^1 are the electron Fermi level in one semiconductor and the hole Fermi level in the other semiconductor, respectively. The recombination current J_{rec} can also be computed from the total number of recombination events occurring in the sample per unit time and unit surface area. The results are obtained by averaging data over many statistically-independent simulations.

Results and discussion

SPV transients

Surface photovoltage (SPV) transients have been computed by means of the present model for different band alignments and

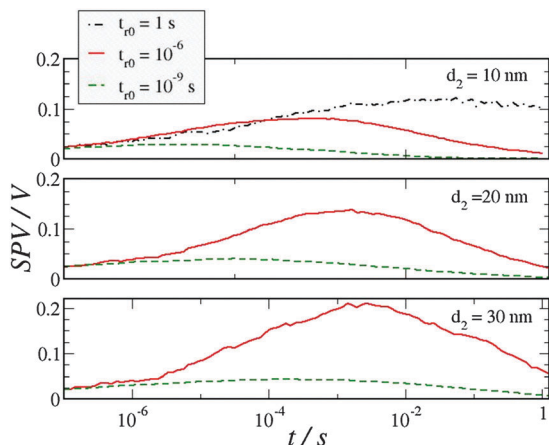


Fig. 2 SPV transients from RWNS calculations for different values of the thickness of the absorber and the recombination frequency ($1/t_0$). The parameters used in the simulations are n_0 (initial pair density) = $8 \times 10^{17} \text{ cm}^{-3}$, $\Delta E_c = -0.1 \text{ eV}$, $E_{g1} = 3.2 \text{ eV}$, $E_{g2} = 1.5 \text{ eV}$, $d_1 = 10 \text{ nm}$, $T_{01} = T_{0p} = 1161 \text{ K}$, $T = 300 \text{ K}$, $t_{0n} = t_{0p} = 10^{-12} \text{ s}$, $\alpha_1 = \alpha_0 = 1 \text{ nm}$ and $a_1 = 1 \text{ nm}$.

band offsets. In Fig. 2 examples of SPV curves can be found. In these calculations a value of $t_0 = 10^{-12} \text{ s}$ has been used, which is found to reproduce in a realistic way the time span of SPV transients in TiO₂ nanostructured electrodes.³⁰ Band gaps of $E_{g1} = 3.2 \text{ eV}$ and $E_{g2} = 1.5 \text{ eV}$ have been used to model TiO₂ and absorber, respectively. The results show that simulated SPV curves have two well-differentiated parts when charge separation is produced. Thus, absolute values of the SPV tend to increase at the beginning of the simulation due to diffusion and charge separation through the heterojunction at shorter times. As a consequence, an absolute maximum is obtained at a certain time, which, in principle, depends on several factors, such as the energy disorder or the band offset of the system. After that, a decay curve appears at longer times as a result of recombination events inside each semiconductor or across the interface.

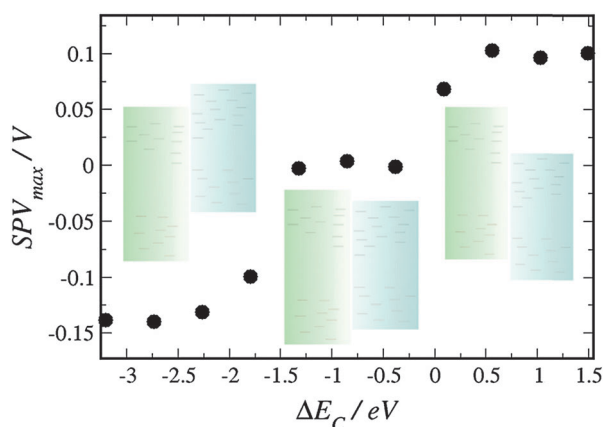


Fig. 3 Maximum surface photovoltage versus band-offset in a disordered heterojunction as obtained from RW calculations with Miller–Abrahams hopping rates and a tunnelling recombination mechanism. The following parameters have been used for the calculations: n_0 (initial pair density) = $2.4 \times 10^{18} \text{ cm}^{-3}$, $E_{g1} = 3.2 \text{ eV}$, $E_{g2} = 1.5 \text{ eV}$, $d_1 = d_2 = 10 \text{ nm}$, $T_{01} = T_{02} = 1161 \text{ K}$, $T = 300 \text{ K}$, $t_{0n} = t_{0p} = 10^{-12} \text{ s}$, $\alpha_1 = \alpha_0 = 1 \text{ nm}$ and $a_1 = 1 \text{ nm}$.

In Fig. 3, values of the peaks of the SPV curves for different band offsets are reported. The simulation shows that the SPV peak starts to be negative and becomes larger as the band offset is increased. Negative values of SPV are expected if we take into account that these cases correspond to values of E_c and E_v that make holes move to the first semiconductor, while forcing electrons to stay in the absorber. When $\text{SPV} > 0$ the charge separation occurs in the opposite direction while no significant charge separation takes place when E_c and E_v are similar. The different band alignments are presented in the inset of Fig. 3. In the two first cases we have a *Type-II heterojunction* while intermediate values of E_c correspond to a *Type-I heterojunction*. The fact that the SPV maxima increase for larger band offsets is an experimental observation that has been reported several times in the literature.⁶¹ It is interesting to note a saturation effect appearing at a certain value of the relative band positions. This seems to be related to a maximum value of the open-circuit voltage (V_{oc}) that can be attained in a solar cell based on a heterojunction for a given degree of energy disorder.

A systematic study of the absorber thickness, the initial charge density and the recombination frequency dependence of the SPV can be found in the ESI† (Fig. S1). The results in accordance with experiments can be observed in all cases, such as the linear dependence between the SPV maxima and the charge density on a log-log scale with an exponent close to unity.^{62,63}

Bulk heterojunction solar cells at open-circuit

A scheme with the parameters used to simulate an archetypical BHJ solar cell is shown in the ESI† (left panel of Fig. S2). Following ref. 39, we have considered that it is kinetics and diffusion, instead of a built-in electric field, that provide the photocurrent and the photovoltage in this type of solar cell under working conditions. Thus, the aim of this study is to test whether those assumptions reproduce the experimental phenomenology. It is important to bear in mind that a built-in electrical field influences dissociation of excitons and can provide an additional driving force for transport by drift.^{64–66} However, as said, we intend to check whether the assumption of neglecting electrical fields, leads to the right phenomenology so that the impact of the electrical field can be critically analyzed.

As previously described, the open-circuit voltage can be calculated from the splitting of Fermi levels for electrons in the acceptor material and holes in the donor material, respectively, in accordance with eqn (8). The same procedure is also used to compute open-circuit voltages of QD-sensitized solar cells. In Fig. 4 energy histograms of electron and hole occupancies for a specific set of parameters are shown. It is observed that when a stationary state is reached, signalled by constant electron and hole densities (see inset of Fig. 4), carrier occupancies fit well to the predictions of Fermi–Dirac statistics. In this way, Fermi levels can be estimated from these energy histograms by fitting to the Fermi–Dirac distribution such that the open-circuit photovoltage can be extracted from eqn (8).

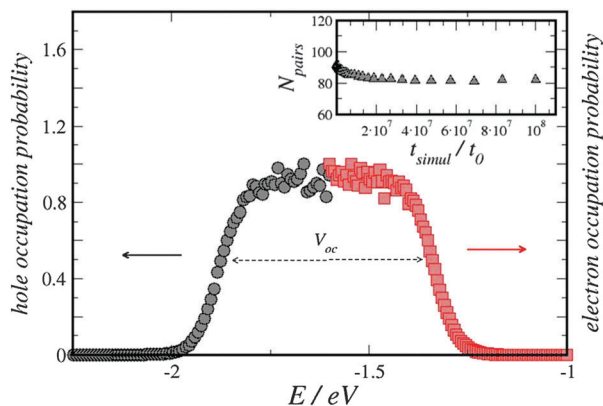


Fig. 4 Occupation probability of energy levels. It is observed that when a stationary state is reached electron and hole occupancies are given by Fermi–Dirac statistics. The open-circuit photovoltage is obtained from the splitting of the Fermi levels ($V_{oc} \sim 0.53$ eV in this case).

Table 1 Simulation parameters

	BHJ		QDSC	
	Polymer	PCBM	CdSe	TiO ₂
E_g (eV)	1.85	1.7	2.37	3.20
E_c (eV)	−3.25/variable	−3.90	−2.87	−3.50
E_v (eV)	−5.10/variable	−5.60	−5.24	−6.70
α_i (nm)	2	2	1	1
α_L (nm)	2	2	1	1
d (nm)	40	40	10	10
N_i (cm ^{−3})	10 ²⁷	10 ²⁷	10 ²⁷	10 ²⁷
T (K)	300	300	300	300
T_{on} (K)		500		1161
T_{op} (K)	500		Varied	
t_0 (ps)	1	1	1	1

Specifically, we have used the values of the band positions in order to study a typical BHJ solar cell as shown in Table 1. We have adjusted the recombination prefactor time t_{ro} at 1 sun to reproduce realistic open-circuit voltages in BHJ solar cells.^{4,67}

In BHJ solar cells it is well known that the open-circuit voltage is found to depend linearly on the band offset between the acceptor and the donor. However, an empirical shift of 0.3–0.5 eV with respect to the band offset (electrical gap) is normally found.^{4,68} With the aim of checking the origin of those features, the open-circuit voltage has been computed by means of eqn (8) as a function of the illumination intensity. The results can be found in Fig. 5. First of all, we can observe that values of the open-circuit voltage are effectively smaller than the difference between the LUMO of the acceptor and the HOMO of the donor in all cases, which is a common experimental observation.⁴ Moreover, a logarithmic dependence of the open-circuit voltage with respect to light intensity is observed, as described in eqn (4). These simulation results confirm the theoretical predictions of ref. 39. From the simulated V_{oc} values the β -parameter can be determined by fitting to eqn (4). A value of $\beta = 0.62$ for a characteristic temperature of $T_{on} = T_{op} = 500$ K is obtained.

The fact that $\beta < 1$ evidences non-ideal behavior, related to the extent of energy disorder, given by $k_B T_0$, in agreement with

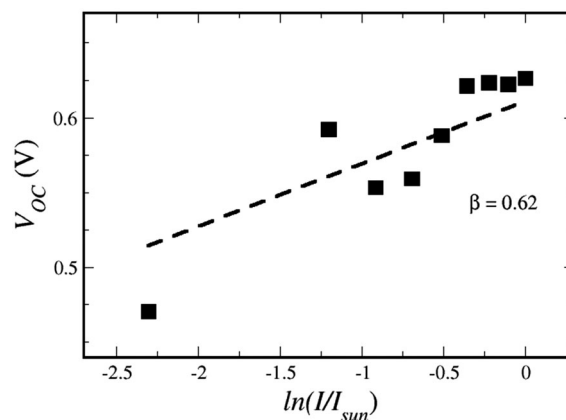


Fig. 5 Open-circuit voltage as a function of the illumination intensity as obtained from splitting of Fermi levels in the RW simulations (squares). The dashed line was obtained by fitting to eqn (4). The parameters used correspond to BHJ values indicated in Table 1. The recombination pre-factor in eqn (7) has been adjusted to reproduce the experimental V_{oc} at 1 sun.

recent studies.^{18,69} To achieve realistic values of the open-circuit voltage and the β -parameter a characteristic temperature of 500 K is required. This is in agreement with a recent report in which a tail state with Urbach energy of $E_u = 47$ meV is considered to account for the experimental observations.²¹

A study of the dependence of the open-circuit voltage on the use of different donor–acceptor combinations in BHJ has also been carried out. In this case, we have followed a recent work by Feng He and Luping Yu⁴ to reproduce experimental open-circuit voltages for different polymer–fullerene combinations. In this particular case, we have considered the same fullerene as acceptor material in all cases while different polymers have been used as donor material according to Table 1 in ref. 4. The calculation has been calibrated by adjusting the recombination pre-factor t_{ro} in eqn (7) and the width of the system so that the open-circuit voltage reported for the first polymer (PTB1) could be accurately reproduced ($V_{oc} = 0.58$ V). Having adjusted this parameter, the rest of the parameters have been kept constant in order to isolate the effect of the offset between the donor and acceptor materials from other features, such as morphology or structure. The parameters for the PCBM in this calculation are the same as shown in Table 1.

The behavior of the open-circuit voltage for different band alignments is shown in Fig. 6. Open-circuit voltages are obtained and represented as a function of the HOMO level of the donor semiconductor. Although the same trend can be obtained from very simple arguments,⁷⁰ it is demonstrated that the RW disordered heterojunction model presented here can reproduce experimental open-circuit voltages for different donor–acceptor combinations by only taking the energy alignment into account. This confirms that, although the morphology can influence open-circuit voltages, resulting in a reduction of 200–300 mV,⁶⁷ still band alignment effects are those determining the suitability of a specific blend.

The effect of the temperature on the open-circuit voltage of bulk heterojunction solar cells has also been addressed.

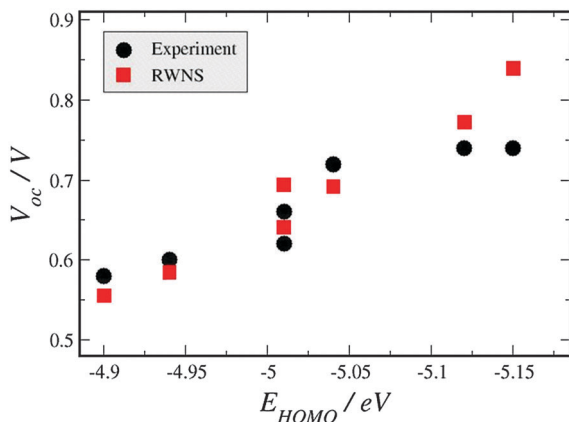


Fig. 6 Open-circuit voltage as a function of the highest occupied molecular orbital (HOMO) energy of the donor material as obtained by RW simulations (red squares) and experimentally as reported in ref. 2 (grey circles). The parameters used in the simulations are those indicated in Table 1 for a BHJ solar cell.

According to recent reports, the open-circuit voltage decreases when the temperature is raised.⁶⁰ This feature is also accomplished by the model as shown in the ESI† (Fig. S4) for two different degrees of illumination.

The ability of the model to reproduce some experimental features implies that a distance-dependent tunnelling recombination mechanism without energy factors seems to be sufficient to account for the functioning of a disordered heterojunction. Bearing this in mind, it is interesting to study the scope of recombination in a BHJ solar cell and to clarify whether recombination occurs only at short distances between adjacent molecules or not. For this reason, we have tried to establish the role that the recombination distance, α_0 , in eqn (7) plays in the open-circuit voltage. This is studied by carrying out calculations for various α_0 . The results are shown in the left panel of Fig. 7. We observe a strong dependence of the open-circuit voltage on the recombination radius. Taking into account that the experimental values are commonly higher than 0.5 V, this observation indicates that the recombination distance has to be small in the real devices. This fact is also supported by the well-known⁷¹ influence of the morphology of the devices on the V_{oc} , which suggests that it is the area of contact between the two semiconductors that determines the overall recombination rate.

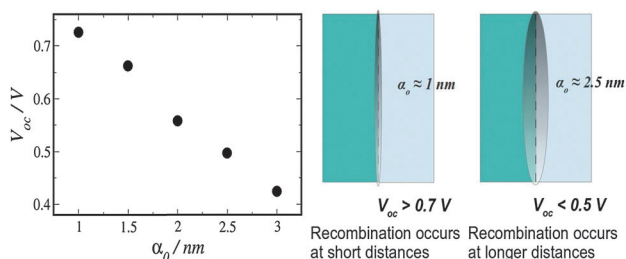


Fig. 7 Left panel: open-circuit voltage as a function of the recombination radius appearing in eqn (7) obtained by RW simulation. The parameters used in the calculations are shown in Table 1. Right panel: a scheme of the process of recombination as a function of recombination distance.

Quantum dot-sensitized (QDSC) solar cells and non-ideality

A scheme including the parameters used to simulate QDSC is shown in the ESI† (right panel of Fig. S2). As explained in the introduction, it is assumed that both the open-circuit voltage between external contacts and the measured recombination current are limited by recombination kinetics across the TiO_2/QD interface only. In addition, we have considered that the Fermi level in the absorber, *i.e.* the QD, is equilibrated with the redox electrochemical potential in the electrolyte. Furthermore, only surface localized states are considered in the QD modelled *via* an exponential distribution.

The parameters used for a TiO_2/CdSe solar cell are shown in Table 1.¹⁷ The recombination prefactor time τ_{r0} has been adjusted to reproduce the experimental V_{oc} at 1 sun⁷² as explained previously.

With these parameters, RW calculations have been carried out to determine the open-circuit voltage as a function of the illumination intensity for various characteristic temperatures of the absorber. To calculate accurate open-circuit voltages in systems with a low number of particles at steady state, the occupation histograms were re-normalized to a common value. The results of the open-circuit voltage as a function of the illumination intensity are found in the ESI† (Fig. S5). The recombination current J_{rec} has also been computed as a function of the illumination intensity. The results for this are plotted *versus* the simulated open-circuit voltage (obtained from the splitting of the Fermi levels, as explained previously) in Fig. 8. As expected, an exponential dependence of the recombination current is found, as predicted by eqn (3).

A striking feature of the results provided by the simulation is that the β -parameter obtained from fitting to eqn (3) is lower than 0.5 for all cases considered. Likewise, it decreases when the energy disorder of the QD is increased. The same trend is found for the open-circuit voltage. Values of β smaller than 0.5 has been observed in actual QDSC.⁷² In this context, it has been pointed out in a recent report by Hod *et al.*⁷³ that the performance of QDSC is controlled by recombination between the

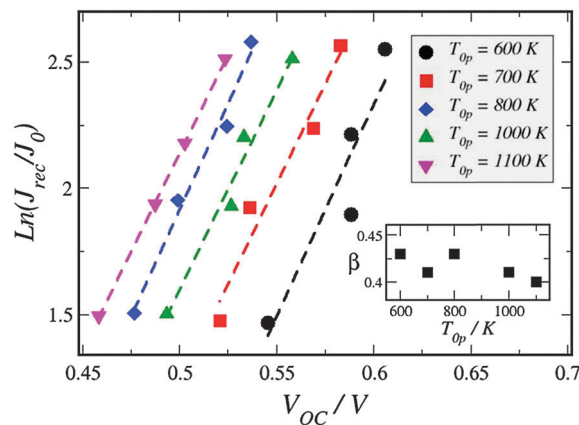


Fig. 8 Recombination current as a function of the open-circuit voltage for various characteristic temperatures of the QD (absorber semiconductor). Simulation data are found in Table 1. The dashed lines were obtained by adjusting to eqn (3). Extracted values of the β -parameter as a function of the characteristic temperature of the QD are shown in the inset.

n-type semiconductor and the QD through localized states at the interface. Hence, the calculations reported here show that a simple recombination mechanism as that given by eqn (7), *i.e.*, an energy-independent recombination at the TiO₂/QD interface, is capable of reproducing this experimental feature.

To rationalize the simulation results, a simple analytical expression for the β -parameter has been derived. To do so, we obtain the recombination current by integration in the energy scale, using $g_n(E_c)$ and $g_p(E_v)$ as the exponential distributions defined in eqn (5) and a recombination frequency ν_{rec} given by the inverse of eqn (7). By applying the zero-temperature limit of the Fermi–Dirac distribution, the following equation is obtained

$$J_{\text{rec}} = qL\nu_{\text{rec}}N_1^2 \exp\left[\frac{E_v - E_{\text{Fp}}}{K_B T_{0p}}\right] \exp\left[\frac{E_{\text{Fn}} - E_c}{K_B T_{0n}}\right] \quad (9)$$

It has to be noted that since ν_{rec} does not contain an energy-dependence, it does not enter the integration. This is in fact a simplified procedure of that required when using an energy dependent charge transfer mechanism $\nu_{\text{rec}}(E)$, such as that given by the Marcus model. The latter was considered by Bisquert and coworkers²⁴ for the case of a DSC, whereby $\beta = 0.5 + \alpha$ is obtained when a large reorganization energy is assumed in the analytical calculations.¹⁹

Interestingly, when both characteristic temperatures are assumed to be equal ($T_{0n} = T_{0p} = T_0$) the following formula is obtained

$$J_{\text{rec}} = J_0 \exp\left(\frac{\alpha(E_{\text{Fn}} - E_{\text{Fp}})}{k_B T}\right) \quad (10)$$

with $J_0 = qL\nu_{\text{rec}}N_1^2 \exp(\alpha(E_v - E_c)/k_B T)$ and $\alpha = T/T_0$. This assumption would imply that the variation of the recombination current with respect to the voltage and temperature, as shown in eqn (3), is controlled by a unique distribution of surface traps. Eqn (10) shows that $\beta = \alpha$ when it is assumed that the energy disorder is of the same order in both inorganic semiconductors. This result seems plausible as realistic values of the characteristic temperature in disordered heterojunctions correspond to $\alpha = 0.3$ – 0.5 , which can thus explain similar experimental values of β in QDSC. Equal values of the characteristic temperature in both semiconductors have been considered in this work in both Fig. 5 and in ESI† (Fig. S3). In agreement with this theoretical description, simulated values of the β -parameter are found to be very close to the α -parameter in all cases. The theory can easily be extended to the case in which T_{0n} is very large. In that situation, the voltage dependence contained in eqn (10) is only determined by the energy distribution of the absorber, in accordance with the simulation results presented in Fig. 8.

Conclusions

A disordered semiconductor heterojunction model based on random walk numerical simulations has been designed and coded. The model is quite general and, therefore, allows for interpretation of a variety of charge transfer processes

occurring at interfaces of many types of solar cells, such as BHJ or nanostructured solar cells sensitized with inorganic semiconductors.

The following features are found to be correctly reproduced:

- (1) The model predicts that charge separation (SPV) in heterojunctions increases with the band-offset.
- (2) The model predicts a linear dependence between the SPV maximum and the charge density on a log–log scale with an exponent close to unity.
- (3) The model predicts that the V_{oc} in a BHJ solar cell is smaller than the electrical gap $E_{\text{LUMO}} - E_{\text{HOMO}}$ and that the shift is related to the energy disorder.
- (4) The model predicts that there is a linear dependence of V_{oc} versus the logarithm of the illumination intensity (as observed in many solar cells based on disordered heterojunctions).
- (5) The model also predicts the linear dependence between V_{oc} and the electrical gap as observed experimentally in BHJ solar cells, although this is indeed a consequence of point 3 above.
- (6) The model predicts that the V_{oc} decreases when the temperature increases, as observed experimentally.
- (7) The model predicts a strong dependence of V_{oc} on the tunnelling recombination distance, which justifies the strong influence of the morphology on the V_{oc} , as observed experimentally.
- (8) The model predicts the observed dependence of the V_{oc} with respect to illumination and the recombination current with respect to voltage in quantum-dot sensitized solar cells.
- (9) The model predicts a β -parameter smaller than 0.5 as observed in quantum-dot sensitized solar cells.

It is important to mention that the three classes of solar cells that are described in this work have very different characteristics in many details of operation and functioning. However, in this work, rather than focusing on the differences, we focus on common characteristics of these three systems. It is very interesting that a model formulated using specific electron transport and recombination kinetics and selective contacts can describe the most salient features of the three types of solar cell.

In summary, the RWNS technique and its implementation to simulate a disordered heterojunction is found to be suitable to describe correctly charge separation and dynamics in these systems. As the assumptions of the model are based on molecular mechanisms of transport (restricted to diffusion) and recombination, this adequate performance suggests that the study of fundamentals of charge separation in novel solar cells is feasible. Hence, the impact of critical parameters such as morphology, electrical fields, and chemical environment can be more safely assessed using this or similar models.

Acknowledgements

The authors gratefully acknowledge support from MEC under project HOPE CSD2007-00007 (Consolider-Ingenio 2010), Abengoa Research *via* a framework collaboration agreement, and Conacyt under grant number 178510 and the General Coordination of Information and Communications Technologies

(CGSTIC) at CINVESTAV for providing HPC resources on the Hybrid Cluster Supercomputer "Xihucoatl".

Notes and references

- J. Nelson, *The Physics of Solar Cells*, Imperial College Press, 1st edn, 2003.
- Y. Tsunomura, Y. Yoshimine, M. Taguchi, T. Baba, T. Kinoshita, H. Kanno, H. Sakata, E. Maruyama and M. Tanaka, *Sol. Energy Mater. Sol. Cells*, 2009, **93**, 670–673.
- Y. Liang, Y. Wu, D. Feng, S.-T. Tsai, H.-J. Son, G. Li and L. Yu, *J. Am. Chem. Soc.*, 2009, **131**, 56–57.
- F. He and L. Yu, *J. Phys. Chem. Lett.*, 2011, **2**, 3102–3113.
- V. González-Pedro, X. Xu, I. Mora-Seró and J. Bisquert, *ACS Nano*, 2010, **4**, 5783–5790.
- M. A. Hossain, J. R. Jennings, C. Shen, J. H. Pan, Z. Y. Koh, N. Mathews and Q. Wang, *J. Mater. Chem.*, 2012, **22**, 16235–16242.
- J. Burschka, N. Pellet, S.-J. Moon, R. Humphry-Baker, P. Gao, M. K. Nazeeruddin and M. Grätzel, *Nature*, 2013, **499**, 316–319.
- M. M. Lee, J. Teuscher, T. Miyasaka, T. N. Murakami and H. J. Snaith, *Science*, 2012, **338**, 643–647.
- H.-S. Kim, I. Mora-Sero, V. Gonzalez-Pedro, F. Fabregat-Santiago, E. J. Juarez-Perez, N.-G. Park and J. Bisquert, *Nat. Commun.*, 2013, **4**, 2242.
- J. Bisquert, *Phys. Chem. Chem. Phys.*, 2008, **10**, 49–72.
- L. Kronik and Y. Shapira, *Surf. Sci. Rep.*, 1999, **37**, 1–206.
- T. Dittrich, V. Duzhko, F. Koch, V. Kytin and J. Rappich, *Phys. Rev. B: Condens. Matter Mater. Phys.*, 2002, **65**, 15531.
- V. Duzhko, F. Koch and T. Dittrich, *J. Appl. Phys.*, 2002, **91**, 9432.
- V. Y. Timoshenko, V. Duzhko and T. Dittrich, *Phys. Status Solidi A*, 2000, **182**, 227–232.
- T. Dittrich, I. Mora-Sero, G. Garcia-Belmonte and J. Bisquert, *Phys. Rev. B: Condens. Matter Mater. Phys.*, 2006, **73**, 045407.
- I. Mora-Seró, T. Dittrich, G. Garcia-Belmonte and J. Bisquert, *J. Appl. Phys.*, 2006, **100**, 103705.
- F. Fabregat-Santiago, G. Garcia-Belmonte, I. Mora-Seró and J. Bisquert, *Phys. Chem. Chem. Phys.*, 2011, **13**, 9083–9118.
- G. Garcia-Belmonte, *Solid-State Electron.*, 2013, **79**, 201–205.
- J. P. Gonzalez-Vazquez, G. Oskam and J. A. Anta, *J. Phys. Chem. C*, 2012, **116**, 22687–22697.
- R. C. I. MacKenzie, T. Kirchartz, G. F. A. Dibb and J. Nelson, *J. Phys. Chem. C*, 2011, **115**, 9806–9813.
- T. Kirchartz, B. Pieters, J. Kirkpatrick, U. Rau and J. Nelson, *Phys. Rev. B: Condens. Matter Mater. Phys.*, 2011, **83**, 115209.
- C. Groves and N. Greenham, *Phys. Rev. B: Condens. Matter Mater. Phys.*, 2008, **78**, 155205.
- I. Mora-Seró, S. Giménez, F. Fabregat-Santiago, R. Gómez, Q. Shen, T. Toyoda and J. Bisquert, *Acc. Chem. Res.*, 2009, **42**, 1848–1857.
- Q. Wang, S. Ito, M. Gratzel, F. Fabregat-Santiago, I. Mora-Sero, J. Bisquert, T. Bessho and H. Imai, *J. Phys. Chem. B*, 2006, **110**, 25210–25221.
- R. Coehoorn and P. A. Bobbert, *Phys. Status Solidi A*, 2012, **209**, 2354–2377.
- R. G. E. Kimber, E. N. Wright, S. E. J. O'Kane, A. B. Walker and J. C. Blakesley, *Phys. Rev. B: Condens. Matter Mater. Phys.*, 2012, **86**, 235206.
- C. Groves, R. G. E. Kimber and A. B. Walker, *J. Chem. Phys.*, 2010, **133**, 144110.
- V. Dao, J. Heo, H. Choi, Y. Kim, S. Park, S. Jung, N. Lakshminarayan and J. Yi, *Sol. Energy*, 2010, **84**, 777–783.
- I. Mora-Sero, J. A. Anta, T. Dittrich, G. Garcia-Belmonte and J. Bisquert, *J. Photochem. Photobiol., A*, 2006, **182**, 280–287.
- J. A. Anta, I. Mora-Sero, T. Dittrich and J. Bisquert, *J. Phys. Chem. C*, 2007, **111**, 13997–14000.
- J. Nelson, *Phys. Rev. B: Condens. Matter Mater. Phys.*, 2003, **67**, 155209.
- J. Bisquert, *Phys. Chem. Chem. Phys.*, 2003, **5**, 5360–5364.
- Z. Pomerantz, A. Zaban, S. Ghosh, J.-P. Lellouche, G. Garcia-Belmonte and J. Bisquert, *J. Electroanal. Chem.*, 2008, **614**, 49–60.
- J. A. Anta, J. Nelson and N. Quirke, *Phys. Rev. B: Condens. Matter Mater. Phys.*, 2002, **65**, 125324.
- N. Tessler, Y. Preezant, N. Rappaport and Y. Roichman, *Adv. Mater.*, 2009, **21**, 2741–2761.
- D. Mendels and N. Tessler, *J. Phys. Chem. C*, 2013, **117**, 3287–3293.
- J. P. Gonzalez-Vazquez, J. A. Anta and J. Bisquert, *Phys. Chem. Chem. Phys.*, 2009, **11**, 10359–10367.
- A. Hagfeldt and M. Graetzel, *Chem. Rev.*, 1995, **95**, 49–68.
- J. Bisquert and G. Garcia-Belmonte, *J. Phys. Chem. Lett.*, 2011, **2**, 1950–1964.
- J. Nelson, *Phys. Rev. B: Condens. Matter Mater. Phys.*, 1999, **59**, 15374–15380.
- J. A. Anta, I. Mora-Sero, T. Dittrich and J. Bisquert, *Phys. Chem. Chem. Phys.*, 2008, **10**, 4478–4485.
- J. A. Anta, *Energy Environ. Sci.*, 2009, **2**, 387–392.
- J. Nelson and R. E. Chandler, *Coord. Chem. Rev.*, 2004, **248**, 1181–1194.
- H. Bässler, *Phys. Status Solidi B*, 1993, **175**, 15–56.
- B. Movaghar, M. Grunewald, B. Ries, H. Bässler and D. Wurtz, *Phys. Rev. B: Condens. Matter Mater. Phys.*, 1986, **33**, 5545–5554.
- M. Silver, G. Schoenherr and H. Baessler, *Phys. Rev. Lett.*, 1982, **48**, 352–355.
- S. D. Baranovskii, A. L. Efros, B. L. Gelmont and B. I. Shklovskii, *J. Phys. C: Solid State Phys.*, 1979, **12**, 1023–1034.
- N. Kopidakis, K. D. Benkstein, J. van de Lagemaat, A. J. Frank, Q. Yuan and E. A. Schiff, *Phys. Rev. B: Condens. Matter Mater. Phys.*, 2006, **73**, 045326.
- K. D. Benkstein, N. Kopidakis, J. van de Lagemaat and A. J. Frank, *J. Phys. Chem. B*, 2003, **107**, 7759–7767.
- A. Petrozza, C. Groves and H. J. Snaith, *J. Am. Chem. Soc.*, 2008, **130**, 12912–12920.
- J. Nelson, S. A. Haque, D. R. Klug and J. R. Durrant, *Phys. Rev. B: Condens. Matter Mater. Phys.*, 2001, **63**, 6320.
- N. Kopidakis, K. D. Benkstein, J. van de Lagemaat and A. J. Frank, *J. Phys. Chem. B*, 2003, **107**, 11307–11315.

- 53 D. Monroe, *Phys. Rev. Lett.*, 1985, **54**, 146–149.
- 54 J. Bisquert, F. Fabregat-Santiago, I. Mora-Sero, G. Garcia-Belmonte, E. M. Barea and E. Palomares, *Inorg. Chim. Acta*, 2008, **361**, 684–698.
- 55 J. Orenstein and M. Kastner, *Phys. Rev. Lett.*, 1981, **46**, 1421–1424.
- 56 J. Orenstein and M. Kastner, *Phys. Rev. Lett.*, 1981, **46**, 1421.
- 57 V. Stehr, *Phys. Rev. B: Condens. Matter Mater. Phys.*, 2011, **83**, 155208.
- 58 L. J. A. Koster, S. E. Shaheen and J. C. Hummelen, *Adv. Energy Mater.*, 2012, **2**, 1246–1253.
- 59 M. Hilczner and M. Tachiya, *J. Phys. Chem. C*, 2010, **114**, 6808–6813.
- 60 G. Garcia-Belmonte, *Sol. Energy Mater. Sol. Cells*, 2010, **94**, 2166–2169.
- 61 I. Mora-Seró, D. Gross, T. Mittereder, A. A. Lutich, A. S. Sussha, T. Dittrich, A. Belaidi, R. Caballero, F. Langa, J. Bisquert and A. L. Rogach, *Small*, 2010, **6**, 221–225.
- 62 V. Y. Timoshenko, V. Duzhko and T. Dittrich, *Phys. Status Solidi A*, 2000, **182**, 227–232.
- 63 T. Dittrich, S. Bonisch, P. Zabel and S. Dube, *Rev. Sci. Instrum.*, 2008, **79**, 113903.
- 64 L. J. A. Koster, E. C. P. Smits, V. D. Mihailetschi and P. W. M. Blom, *Phys. Rev. B: Condens. Matter Mater. Phys.*, 2005, **72**, 085205.
- 65 C. Deibel, T. Strobel and V. Dyakonov, *Phys. Rev. Lett.*, 2009, **103**, 036402.
- 66 C. Deibel and V. Dyakonov, *Rep. Prog. Phys.*, 2010, **73**, 096401.
- 67 D. Credgington and J. R. Durrant, *J. Phys. Chem. Lett.*, 2012, **3**, 1465–1478.
- 68 A. Wilke, J. Endres, U. Hörmann, J. Niederhausen, R. Schlesinger, J. Frisch, P. Amsalem, J. Wagner, M. Gruber, A. Opitz, A. Vollmer, W. Brütting, A. Kahn and N. Koch, *Appl. Phys. Lett.*, 2012, **101**, 233301.
- 69 J. C. Blakesley and D. Neher, *Phys. Rev. B: Condens. Matter Mater. Phys.*, 2011, **84**, 075210.
- 70 M. C. Scharber, D. Mühlbacher, M. Koppe, P. Denk, C. Waldauf, A. J. Heeger and C. J. Brabec, *Adv. Mater.*, 2006, **18**, 789–794.
- 71 J.-L. Brédas, D. Beljonne, V. Coropceanu and J. Cornil, *Chem. Rev.*, 2004, **104**, 4971–5004.
- 72 V. González-Pedro, X. Xu, I. Mora-Seró and J. Bisquert, *ACS Nano*, 2010, **4**, 5783–5790.
- 73 I. Hod, V. González-Pedro, Z. Tachan, F. Fabregat-Santiago, I. Mora-Seró, J. Bisquert and A. Zaban, *J. Phys. Chem. Lett.*, 2011, **2**, 3032–3035.